ARTICLE

Received 00th January 20xx,
Accepted 00th January 20xx

DOI: 10.1039/x0xx00000x

Cu boosting the collaborative effect of Ni and H^+ in alloyed NiCu/saponite catalysts for the hydrogenolysis of glycidol

Fiseha Bogale Gebretsadik,[a] Javier Ruiz-Martinez,[b, c] María Dolores González,[a] Pilar Salagre,[a] and Yolanda Cesteros[a*]

The effect of copper on various acid saponite supported Ni-Cu bimetallic catalysts, prepared with different Ni:Cu ratios, was studied for the liquid phase hydrogenolysis of glycidol on a batch reactor at 393 and 453 K. Characterization of the catalysts showed that Ni and Cu are in intimate contact since XRD measurements evidenced the formation of an alloy. H_2 chemisorption results revealed that the measured metallic area progressively decreased with an increase in the wt % of copper. In the presence of high metal activity (higher Ni wt %), the formation of 1,2-propanediol (1,2-PD) outweighed, while acid activity led to the formation of dimerization and oligomerization products. The addition of Cu and the increase of the reaction temperature decreased the diol formation but boosted the 1,3-PD/1,2-PD ratio. This could be explained by an improvement of the collaborative effect between metal Ni and H^+ of the saponite. Therefore, the presence of the appropriate amount of Cu allowed the control of the hydrogenation capacity of Ni, and enhanced the collaborative effect of Ni and H^+ favouring the formation of 1,3-propanediol with respect to 1,2-propanediol.

1. Introduction

Biomass valorization is crucial for the sustainability of our society [1,2] and aids to solve the environmental impact related to the use of fossil fuels.[3,4] One of the most explored valorization processes at the academic and industrial level is the conversion of renewable oils into biodiesel. Additionally, this chemical process also produces glycerol in 10 % yield. The rapid growth of the biodiesel industry results in a glycerol oversupply, which negatively impacts the market value of this product.[5-9] To make the biodiesel industry more economically competitive, various innovative processes were developed to transform glycerol to other added value chemicals.[8,10]

Selective hydrogenolysis of glycerol to 1,3-propanediol (1,3-PD) is a valorization route especially attractive due to the high cost of the current industrial processes.[11] 1,3-PD is an important monomer in the synthesis of polypropylene terephthalate (PPT),[12] a polymer that displays excellent chemical resistance, light stability, elastic recovery and dyeability.[13,14] The hydrogenolysis of glycerol to 1,3-PD has been attempted by different research groups.[10,15-23] The most interesting results in terms of 1,3-PD yield were obtained when expensive noble metal-based catalysts were used at harsh reaction conditions and long reaction time.[10,12,18-23]

Glycidol could be an alternative to glycerol for propanediol production since is a highly reactive molecule that could be readily obtained in one step from the reaction of glycerol and dimethyl carbonate[24,25] or from epichlorohydrin industry wastes.[26] Epoxides can undergo ring opening reactions in the presence of acid solids,[27-29] and supported metal catalysts.[30-32] Isomerization and hydrogenolysis of epoxides to aldehydes, ketones or alcohols using different supported metal catalysts has been previously described. [30-32] Tetrahydrofurfuryl alcohol (THFA) was hydrogenolyzed to 1,5-pentanediol using Mo and Re modified Rh[33-35] and Re modified Ir catalysts supported on SiO_2 or C.[36] Dumesic et al. reported the hydrogenolysis of secondary C-O bonds of several cyclic ethers.[37] The authors claimed that these reactions require a bifunctional catalyst. In this way, acidic O-H groups on ReO_x activated the cyclic ether.

Saponite, $M_{x-y/n}[(Mg_{6-y}Al_y)^{Td}[(Si_{8-x}Al_x)^{Oh}.O_{20}(OH)_4].nH_2O$, is a trioctahedral clay of the smectite group containing an octahedral (Oh) sheet of MgO between tetrahedral (Td) sheets of SiO_4. Isomorphous substitution of Si by Al generates a negative layer charge, which should be compensated by interlayer hydrated cations (M^{n+}). When the interlayer cation is exchanged by H^+, the saponite has Brønsted acidity and can be used as support with acid properties.

The use of Ni as a cheaper alternative to noble metals in the hydrogenolysis of biomass-derived polyols has attracted a great attention.[38-40] Ni has high hydrogen activation capacity and could be used for the production of alcohols from

[a] Universitat Rovira i Virgili, Departament de Química Física i Inorgànica, C/ Marcel·lí Domingo 1, 43007 Tarragona, Spain
[b] Inorganic Chemistry and Catalysis, Debye Institute of Nanomaterials, Utrecht University, Universiteitsweg 99, 3584 CG Utrecht, The Netherlands.
[c] KAUST Catalysis Center (KCC). King Abdullah University of Science and Technology Bldg.3, Level 4, Room 4275, Thuwal 23955-6900, Saudi Arabia.

† Footnotes relating to the title and/or authors should appear here.
Electronic Supplementary Information (ESI) available: [details of any supplementary information available should be included here]. See DOI: 10.1039/x0xx00000x

epoxides. The mechanism of the ring opening depends on several factors, such as the presence of Brønsted acidity and metals.[37] The control of the reaction pathway will be fundamental for the production of 1,3-PD or 1,2-PD from glycidol. In previous works, we achieved 29 % of yield to 1,3-PD from the hydrogenation of glycidol over an acid saponite supported Ni catalyst, that further increased to 46.1% over a ReOx modified supported Ni catalyst.[41, 42] More recently, Y. Sun et al. reported a yield to 1,3-PD of 50.4 % using a carbon film encapsulated Co catalyst.[43] The authors concluded that the formation of 1,3-PD was sensitive to the amount of adsorbed hydrogen, being favoured at moderate adsorption values. Taking into account this idea, the aim of this work was to delve into the study of the effect of adding a second metal with less hydrogen adsorption capacity, such as Cu, on the catalytic activity of supported Ni-Cu bimetallic catalysts, prepared with different Ni:Cu ratios, for the hydrogenolysis of glycidol. The Ni activity is strongly dependent on Ni nanoparticle size.[44] The addition of Cu, as a second metal, can be a good option to decrease the Ni particle size, since the Cu can reduce the ensemble size of Ni by formation of an alloy.[45] Cu is a less-active metal but can be an efficient catalyst for a selective C-O bond hydrogenolysis.[46,47] Some selected catalysts will be also tested at higher reaction temperature to see the effect of this parameter on the catalytic results.

2. Experimental

2.1. Preparation of the catalysts

Several supported Ni-Cu catalysts, with different Ni:Cu ratios, were prepared by the incipient wetness impregnation method using a H-saponite (S), the synthesis of which was previously reported,[48] as support. One H-saponite supported monometallic Ni catalyst and one H-saponite supported monometallic Cu catalyst were also prepared as reference for comparison. For catalyst preparation, 1 g of support was introduced into a round bottom flask. A calculated volume of 0.5 M nickel or copper nitrate solution in ethanol, to make supported catalysts at 30 wt % Ni or Cu loading, was poured uniformly over the support. For the Ni-Cu bimetallic catalysts, calculated amounts of $Ni(NO_3)_2$ and $Cu(NO_3)_2$, to make a Ni-Cu catalyst at Ni:Cu wt % ratio (9:1), (6:1), (3:1), (1:1) and (1:3), were dissolved in ethanol to make a 0.5 M solution with respect to the total moles of the metal precursors. The solution was transferred uniformly into the round bottom flask with the support. The solvent was removed by rotary evaporation. The samples were dried in an oven at 363 K overnight, calcined in static air from room temperature at 10 K/min to 723 K and maintained at this temperature for 5 h, and reduced in a tubular reactor under hydrogen flow (75 mL/min) at 623 K for 6 h. The monometallic catalysts were named as Ni/S and Cu/S. In the case of the bimetallic catalysts, the nomenclature was NiCu(X:Y)/S where X, Y represented the relative wt % ratio of Ni and Cu, respectively. One more sample (NiCu(6:1)*/S) was prepared at 40 wt % of total metal loading in a Ni:Cu wt % ratio of 6:1, for comparison. The catalyst precursors were labelled with a P before the name of the catalyst. Several spent catalysts were characterized after reaction and were named by adding –U to the nomenclature of the catalyst.

2.2. Characterization of the catalysts

X-ray diffraction (XRD) patterns of the powdered catalyst samples were recorded on a Siemens D5000 diffractometer equipped with a CuKα radiation ($\lambda \approx 1.5406$ Å) source. Measurements were done in 5-70° 2θ diffraction angles, with an angular step of 0.05° and at a rate of 3s per step. Crystalline phases were identified by cross comparison of the diffractogram of the sample with a reference data from international center for diffraction data (ICDD, release 2004) files. TOPAS 4.1 software was used to fit the diffractograms with the Rietveld method and the crystal structure of each phase. The average crystallite size was calculated as a mean value from all the diffracted peaks once the instrumental contribution to the peaks width was removed. The cell parameters calculated from the refined diffractogram were used to examine the formation of Ni-Cu alloy and to determine the stoichiometry of constituent metals in the alloy.

N_2 adsorption-desorption analysis of the catalyst precursors and spent catalysts were performed on Quadrasorb SI surface analyser at liquid nitrogen temperature (77 K) to determine the BET area, pore volume and average pore size. Before measurement, samples were degassed overnight at 383 K. The spent catalysts were degassed at higher temperature (573 K) for 3 h in order to remove the high boiling point solvent, sulfolane (b.p. 558 K), used during the catalytic reaction that could not be removed by aqueous washing. Specific surface area was determined by applying the BET method and the pore size distribution was estimated from BJH method.

TEM characterization of the catalysts was done using a JEOL 1011 transmission electron microscope operating at an accelerating voltage of 100 kV and magnification of 200 k. The catalyst powder (0.1 mg) was dispersed in ethanol (50 µL) with the aid of ultrasounds. Then, the suspension was placed on a carbon coated copper grid and air dried.

The temperature-programmed reduction profile of the catalyst precursors was analyzed by an Autochem AC2920 Micrometric apparatus. A sample calcined beforehand (100 mg) was introduced into the sample tube equipped with thermal conductivity detector. The sample was heated from room temperature to 1173 K at a rate of 10 K/min under a flow of 5% H_2 in argon (50 mL/min). The amount of hydrogen consumed was monitored by a TCD detector. The measured metallic area was calculated applying the chemisorption factor of copper for Cu/S and the chemisorption factor of nickel for Ni/S and NiCu catalysts taking into account the low hydrogen adsorption capacity of copper.

Surface acidity of the catalyst precursors was determined from thermogravimetric analysis (TGA) of their cyclohexylamine (CHA) treated samples following the protocol described by Mokaya et al.[49] The total acidity was equivalent to the amount of cyclohexylamine desorbed at the temperature range of 473-923 K in which the sample without cyclohexylamine treatment

did not show any significant mass loss. [49] The samples without cyclohexylamine treatment were analysed in the same way and used as a blank to account for potential mass loss unrelated to the basic probe molecule. The analysis was conducted in a Labsys Setaram TGA microbalance equipped with a programmable temperature furnace. Each sample was heated under N_2 flow (80 cm^3/ min) from 303 to 1173 K at a rate of 10 K/ min. In all experiments, the amount of sample used was around 100 mg.

The amount of organic material deposited on the spent catalyst was determined by TG analysis. In the analysis, the spent catalyst was dried at 573 K under vacuum for 3 h in order to remove the adsorbed sulfolane solvent used in the catalytic reaction. About 100 mg of the dried samples was put in the sample holder and heated from 303 to 1173 K under air flow (80 cm^3/ min) at a heating rate of 10 K/ min. The same temperature range, as in the acidity determination (523-923 K) was used to determine the percentage of organic product.

2.3. Catalytic Activity

Hydrogenolysis of glycidol was tested in a 50 mL stainless steel autoclave equipped with an electronic temperature controller and a mechanical stirrer. Glycidol (3.77 mL) was dissolved in sulfolane (30 mL) and purged with nitrogen. A freshly reduced catalyst (1 g) was carefully transferred to the reactor under a positive nitrogen pressure to avoid contact with the atmosphere. The reactor was sealed and purged three times with 4 MPa N_2 pressure and three times with 1 MPa H_2 pressure. After performing a leakage test, the temperature of the reaction was set at 393 or 453 K, the stirring at 600 rpm and 1 MPa H_2 was fed. When the temperature in the electronic control reached the final temperature of the reaction, the hydrogen pressure was adjusted at 5 MPa and the reaction time was started (t_o). The reaction was allowed to run for 1 or 4 h while feeding hydrogen on demand. At the end of the reaction (t_f), the reaction mixture was cooled and gaseous reaction products were collected in a gas bag. The reaction products were separated from the catalyst by centrifugation and liquid products were analysed on a Shimadzu GC-2010 chromatograph using a SupraWAX-280 capillary column, 1-butanol as internal standard and a FID detector. Some liquid samples were submitted for GC-MS analysis to identify the unknown products. Conversion and selectivity of the reactions were calculated according to the following equations:

$$Conversion = \frac{(moles\ of\ glycidol\ t_o - moles\ of\ glycidol\ t_f)}{moles\ of\ glycidol\ t_o} * 100\%$$

$$Selectivity\ to\ x\ (\%) = \frac{\text{moles x} * \text{carbon in x}}{moles\ of\ glycidol\ converted * carbon\ in\ glycidol} * 100\%$$

3. Results and Discussion

3.1. Characterization of catalytic precursors

The reducibility of the supported metal oxides was assessed by temperature-programmed reduction. Figure 1 shows the reduction profiles of the catalyst precursors. The reducibility of a metal oxide depends on many factors, such as the nature of the supported metal, its particle size and its interaction with the support.[50] The monometallic Ni catalyst precursor (PNi/S) displayed two reduction peaks: one well-defined peak centered at 770 K and a broad shoulder between 820-1000 K. The lower temperature peak was due to smaller NiO particles whereas the broad peak was assigned to either more aggregated NiO or NiO particles, which had strong interaction with the support. Similarly, PCu/S (Figure 1) exhibited the main reduction peak at 520 K with shoulders between 390-470 and at 557 K. The different contributions can be attributed to CuO particles with different size and support interaction. The presence of Cu and an increase in its wt % ratio progressively shifted the main reduction peak to lower reduction temperatures. For PNiCu(3:1)/S, another small peak, which was shifted even to lower reduction temperature with respect to the monometallic Cu catalyst, appeared at 490 K. This peak was the main reduction peak for samples PNiCu(1:1)/S and PNiCu(1:3)/S. As we will discuss later, this peak could be related to the formation of an alloy. The PNiCu(1:1)/S and PNiCu(1:3)/S samples also showed peaks that shifted to lower reduction temperatures compared to the monometallic PCu/S catalyst precursor. This could be attributed to the higher reducibility of the smaller copper oxide particles obtained in the bimetallic catalysts.[51,52]

The N_2-adsorption results of the support and the catalyst precursors are presented in table 1. The support (S) had specific BET area of 196 m^2/g and pore volume of 0.21 cc/ g. The values of specific BET area and pore volume decreased to 122-112 m^2/g and 0.17-0.12 cc/g, respectively, for the supported catalysts precursors prepared at 30 wt % total metal loading. The value of the specific BET area decreased further to 77 m^2/g for the catalyst prepared at 40 wt % total metal loading. This could be attributed to the occupation of part of

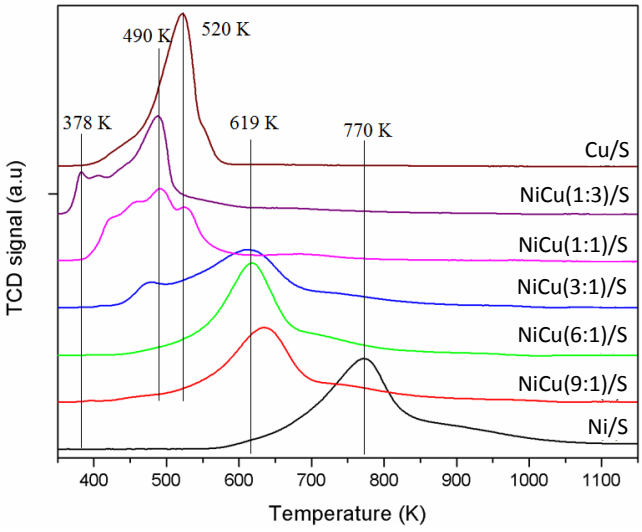

Figure 1: TPR profiles of all the catalyst precursors.

Table 1: Characterization results of the support and catalyst precursors.

Support and catalyst precursors	BET (m^2/g)	Average pore radius (Å)	Pore volume (cc/g)	Acidity (x 10^{-3} eq CHA/g)[a]
S	196	21	0.21	1.33
PNi/S	126	21	0.13	1.21
PNiCu(9:1)/S	129	25	0.13	1.22
PNiCu(6:1)/S	127	23	0.14	1.22
PNiCu(3:1)/S	116	29	0.17	1.19
PNiCu(1:1)/S	116	27	0.17	1.07
PNiCu(1:3)/S	114	30	0.17	1.03
PCu/S	112	29	0.18	1.05
PNiCu(6:1)*/S	77	30	0.15	0.81

[a] Calculated from TGA of adsorbed cyclohexylamine.

the support pore volume by the metal oxide particles. The decrease of the pore volume was more significant when the wt % of the Ni loading increased. A similar result was reported by Obregon and coworkers.[53] They claimed that Ni is preferentially deposited in bigger pores while Cu takes up the external surface.

The total surface acidity of all the catalyst precursors (1.03-1.21 mEq CHA/g) was lower than the acidity of the support alone (1.33 mEq CHA/g), as shown in Table 1. The decrease in the acidity of the catalyst precursors could be explained by the coverage of part of the acid sites with the impregnated metal, as confirmed by the lower surface area of the catalyst precursors compared to the support (Table 1). It was also observed that the surface acidity of the catalyst precursor decreased at higher wt % Cu loading. This could be related to a higher presence of CuO on the external surface.[53]

3.2. Characterization of fresh catalysts

XRD patterns of the catalysts presented the characteristic saponite reflections at 19.4º, 35.6º, 60.5º, 2 θ , due to (110, 020), (201) and (060) planes, respectively, together with metallic phases (Figure 2). For the monometallic Ni catalyst, Ni/S, reflections appeared at 44.5º and 51.9º, 2 θ , corresponding to (111) and (200) planes of metallic nickel without observing significant amounts of the NiO phase. XRD pattern of Cu/S showed reflections at 43.3º and 50.4º, 2 θ , which are assigned to (111) and (200) planes of metallic Cu.

In the case of Ni-Cu bimetallic catalysts, illustrated in Figure 2 b-f, the position of the reflection peaks shifted, depending on the wt % ratios of Ni and Cu, to lower 2 θ angles with respect to the peaks of the supported monometallic Ni catalyst. Accordingly, slight comparable shift in the position of the Ni peak at 44.5º, 2 θ was observed for NiCu(9:1)/S and NiCu/(6:1) samples. Catalyst NiCu(3:1)/S showed further shift and the reflection appeared broader. This could be related to the formation of a Ni-Cu alloy, as previously reported.[45] For the NiCu(1:1)/S and NiCu(1:3)/S catalysts, the peak shift was even more pronounced. Unlike in previous reports[45,47] where the Ni-Cu alloy was more enriched with Cu irrespective of the initial metal ratio, in our case, the stoichiometry of the alloy formation was governed by the atomic ratios of Ni and Cu in

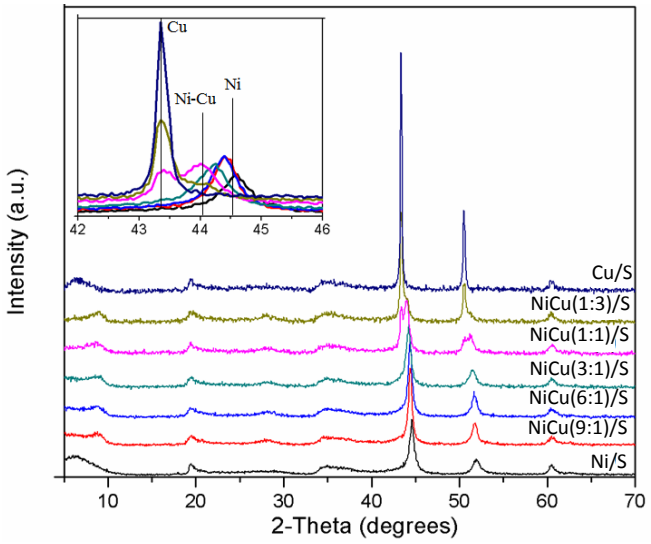

Figure 2: XRD patterns of the catalysts.

the samples. This might be the result of the calcination procedure at 723 K for 5 h that favored good mixing of the metals. In catalysts NiCu(1:1)/S and NiCu(1:3)/S, especially in the later sample, some amount of metallic Cu, which did not form an alloy, was also present.

The cell parameters of the samples were plotted against the atomic ratios of Ni, as shown in Figure 3. The cell parameter clearly showed a tendency to decrease as the Ni content of the alloy increased, as expected from Vegard´s law.[54] As Ni and Cu have the same crystal structure, a continuous solid solution between the two metals can be expected. For catalysts NiCu(9:1)/S, NiCu(6:1)/S, NiCu(3:1)/S and NiCu(1:1)/S, there was a good agreement between the Vegard's law and the cell atomic ratios of Ni and Cu in the sample and the stoichiometry of the alloy were almost identical. In sample NiCu(1:3)/S, probably the surface was enriched with Cu, as confirmed by the deviation of its cell parameter to that would be expected from Vegard´s law. This might be due to thermodynamic reasons whereby the lower surface free energy of Cu, when compared

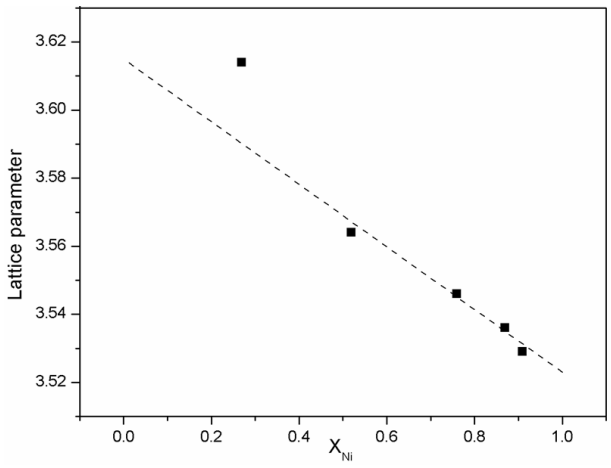

Figure 3: Cell parameter calculated from the XRD patterns as a function of Ni content and Vegard's curve.

Table 2: Characterization of fresh catalysts

Catalysts	Metal crystallite size XRD (nm)	Particle size TEM (nm)	Metallic area [b] (m^2/g sample)
Ni/S	8	15	7.5
NiCu(9:1)/S	12[a]	---	3.4
NiCu(6:1)/S	11[a]	---	2.8
NiCu(3:1)/S	9[a]	14[a]	2.4
NiCu(1:1)/S	11[a] (18)	13[a]	0.4
NiCu(1:3)/S	7[a] (41)	18[a]	0.2
Cu/S	62	95[a]	0.1
Ni-Cu(6:1)*/S	---	---	4.3

[a] Particle size of the Ni-Cu alloy. The values between parentheses correspond to Cu particle size; [b] Measured by Hydrogen chemisorption.

to Ni, led to a enrichment of Cu in the external surface of the bimetallic catalyst.[55] The average crystallite sizes of Ni, Cu or Ni-Cu alloy of the catalysts was determined from their XRD pattern by applying the Scherrer equation (Table 2). Monometallic Ni and Cu catalysts showed particle sizes of 8 and 62 nm, respectively. NiCu(9:1)/S, NiCu(6:1)/S and NiCu(3:1)/S samples had Ni-Cu alloy particle sizes of 12, 11 and 9 nm, in this order. For the other two samples, NiCu(1:1)/S and NiCu(1:3)/S, two types of particles namely, metallic Cu and Ni-Cu alloy were observed. The average crystallite size of the alloy particles was 11 and 7 and the Cu crystallite size was 18 and 41 nm, correspondingly for NiCu(1:1)/S and NiCu(1:3)/S. These results suggest that the formation of a Ni-Cu alloy helps to the dispersion of Cu.

Representative TEM images of some of the catalysts are displayed in Figure 4. TEM micrographies gave direct evidence on the degree of dispersion and homogeneity of the metal particles. The monometallic Ni/S and Cu/S, in figure 4A and 4E,respectively, showed particles with a good size homogeneity. The average particle size of Ni/S (15 nm) was much smaller than Cu/S (95 nm). This is in agreement with the crystallite size calculated from the XRD patterns. NiCu(3:1)/S catalyst, in figure 4B, had similar particle size distribution to that of the monometallic Ni/S. For the other two samples, NiCu(1:1)/S and NiCu(1:3)/S, in figure 4C and 4D, respectively, a more heterogeneous particle size distribution was observed. Small particles, which might correspond to the alloys, and bigger particles of metallic copper were observed. This was in agreement with the XRD pattern discussed previously that showed two distinct peaks for these two samples corresponding to Ni-Cu alloy and metallic Cu.

The metallic area of fresh catalysts, determined from hydrogen chemisorption analysis, is shown in Table 2. Ni/S showed the highest metallic area (7.5 m^2/g). Interestingly, the measured metallic area decreased for the bimetallic catalysts when increasing the wt % of Cu loading. Thus, NiCu(1:1)/S and NiCu(1:3)/S catalysts had a metallic area of 0.4 and 0.1 m^2/g, respectively. The Cu/S catalyst did not show appreciable amount of hydrogen strongly chemisorbed. These results were in agreement with the low hydrogen chemisorption capacity reported for Cu.[56]

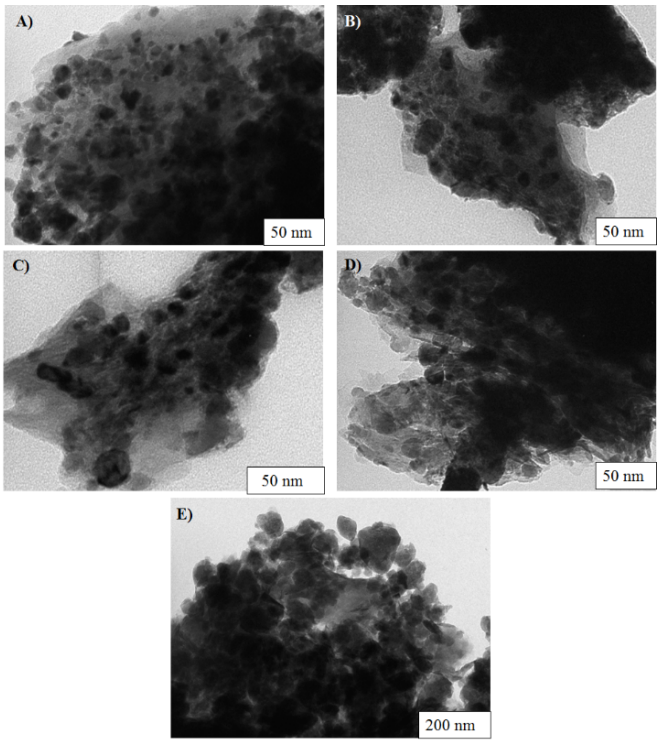

Figure 4: TEM images of A) Ni/S (300 k), B) NiCu(3:1)/S (300 k), C) NiCu(1:1)/S (500 k), D) NiCu(1:3)/S (300 k) E) Cu/S (80 k) catalysts.

3.3. Catalytic Activity

The effect of the type of metal (Ni or Cu) and the relative composition of the two metals in the Ni-Cu bimetallic catalysts on the product distribution of glycidol hydrogenolysis was studied by testing them at 393 K for 4 h. The major products of the reaction identified from GC-MC analysis include 1,3-PD, 1,2-PD, propanol and cyclic dimerization products such as dioxane and dioxolane derivatives. The proposed acid, metal, and acid/metal catalyzed reaction pathways leading to each of the products identified from GC-MS analysis are illustrated in

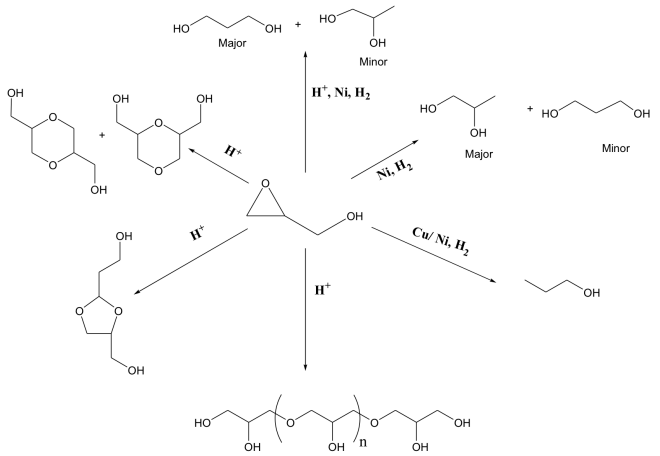

Scheme 1.

Scheme 1: A simplified reaction pathways for acid, Ni/Cu and Ni/Cu

Metal and acid sites promote the formation of 1,3-PD, therefore, we foresee that an intimate between both active sites will be crucial. The acid catalyzed isomerization reaction products, reported by other authors on differently substituted oxiranes,[27,28] were not detected. This might be because acid catalyzed isomerization reaction products of glycidol, the bifunctional 3-hydroxypropionaldehyde or acetol, were unstable under our reaction conditions and could undergo hydrogenation, condensation or oligomerization reactions. The formation of high molecular weight oligomerization reaction products, deposited on the spent catalysts, was confirmed in some catalysts by temperature programed oxidation-thermogravimetric analysis as commented below.

The catalytic activity results of the catalysts tested at 393 K for 4 h are shown in Table 3 and some of them are represented in Figure 5. Ni/S catalyst showed full conversion. However, the conversion values decreased when increasing the wt % of Cu loading in the catalysts. Thus, NiCu(9:1)/S, NiCu(6:1)/S and NiCu(3:1)/S exhibited comparable conversion (78-73 %) whereas conversion decreased further to 56-34 % for NiCu(1:1)/S, NiCu(1:3)/S and Cu/S as the wt % ratio of Cu increased. These conversion values are in good agreement with the measured metallic area, taking into account the similar acidity of the catalysts, and could be explained by the higher hydrogenating capacity of Ni compared to Cu[57] at this comparatively lower reaction temperature. Regarding the product distribution of the catalysts, it was observed that the total diol selectivity decreased and the propanol and dioxane and dioxolane selectivity values increased when increasing the wt % ratio of Cu in the catalysts (Table 3, Figure 5). We propose that diols might be formed mainly by nickel catalyzed hydrogenation, favoring the 1,2-PD formation. However, the 1,3-PD/1,2-PD ratio increased with the increase of Cu. This suggests that it is necessary to modify the activity of Ni in order to promote the collaborative effect between acid and metal sites. The acid activated oxirane ring of the glycidol could favor the cycle opening by the cleavage of the more hindered C2, as has been commented in the literature for other cyclic ethers,[27] favoring the formation of 1,3-PD. The high total diol selectivity values of the catalysts with high Ni wt % ratio confirmed the higher hydrogenating capacity of Ni and

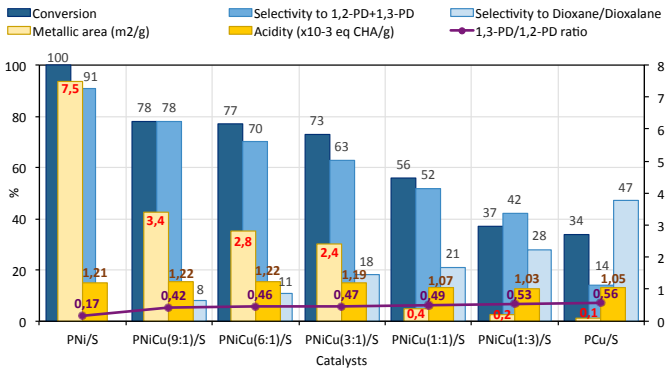

Figure 5. Catalytic Activity results for the hydrogenolysis of glycidol at 393 K for 4 h.

was in agreement with their higher measured metallic area values. In the case of Ni/S catalyst, the lowest, 1,3-PD/ 1,2-PD ratio (0.17) could indicate that its higher metallic area (7.5 m^2/g of catalyst) could led direct hydrogenation without the involvement of acid sites. This could favor the hydrogenolysis of the less sterically hindered primary C-O bond leading to the formation of 1,2-PD. In the other catalysts, in which the metallic areas were moderate or low, the contribution of such direct reactions could be lower and hydrogenolysis, through acid activation, favored 1,3-PD formation.

In the case of propanol, for Ni/S catalyst the selectivity was 3 % and for other catalysts, the selectivity increased progressively when the measured metallic areas decreased and the wt % of Cu in the catalysts increased. This might indicate that the main route for propanol formation was not over hydrogenolysis, as could be expected from the lower activity of Cu and the lower degree of over hydrogenolysis expected at such lower reaction temperature (393 K) for Ni/S (Scheme 1). In the literature, it was suggested that Cu has deoxygenation capacity on epoxide rings[32] at similar reaction conditions as those used in our experiments. Hence, the propanol could be the product of deoxygenation of glycidol to 3-propen-1-ol followed by hydrogenation. The dioxane or dioxolane selectivity increased with a decrease in the metallic area. This suggests that when hydrogenolysis activity is lower, the contribution of acid catalyzed reaction is higher and favors the intermolecular oligomerization and dimerization of the reactions products.

In order to establish the role of acidity in the selective

Table 3: Catalytic activity of all the catalysts at 393 K for 4 h

Catalyst	Conversion (%)	Selectivity (%)						1,3-PD/ 1,2-PD ratio	1,3-PD yield (%)
		1,2-PD	1,3-PD	1,2-PD + 1,3-PD	Propanol	Dioxane/ dioxolane	Others		
Ni/S	100	78	13	91	3	---	6	0.17	13
NiCu(9:1)/S	78	55	23	78	6	8	8	0.42	18
NiCu(6:1)/S	77	48	22	70	12	11	7	0.46	17
NiCu(3:1)/S	73	43	20	63	13	18	5	0.47	15
NiCu(1:1)/S	56	35	17	52	19	21	7	0.49	10
NiCu(1:3)/S	37	28	15	42	23	28	7	0.53	6
Cu/S	34	9	5	14	34	47	5	0.56	2
NiCu(6:1)*/S	70	69	13	82	9	5	4	0.19	9

Table 4: Catalytic activity of selected catalysts at 453 K for 1 h.

Catalyst	Conversion (%)	Selectivity (%)						1,3-PD/ 1,2-PD ratio	1,3-PD yield (%)
		1,2-PD	1,3-PD	1,2-PD + 1,3-PD	Propanol	Dioxane/ dioxolane	Others		
Ni/S	99	57	23	80	14	---	6	0.40	23
NiCu(9:1)/S	96	41	22	63	16	15	6	0.54	21
NiCu(6:1)/S	94	37	21	58	21	15	6	0.57	20
NiCu(3:1)/S	92	32	19	50	22	18	10	0.59	17
NiCu(1:3)/S	82	18	13	31	32	26	11	0.72	11
Cu/S	75	5	4	9	45	31	15	0.80	3
NiCu(6:1)*/S	95	48	21	70	21	4	5	0.44	20

formation of 1,3-PD, the catalytic activity of NiCu(6:1)*/S catalyst with higher total metal loading (40 wt %), was tested at 393 K for 4 h. This catalyst showed the lowest surface acidity (0.81 mEq CHA/ g) among all the catalysts tested probably due to coverage of the acid sites by metal sites and its higher metallic area (4.3 m^2/g of catalyst) compared to NiCu(6:1)/S (2.8 m^2/ g of catalyst). This catalyst showed higher total diol selectivity and lower propanol and dioxane or dioxolane selectivity compared to the other bimetallic catalysts. In addition, the 1,3-PD/ 1,2-PD ratio was the lowest (0.19) of all the bimetallic catalysts. This might suggest that the low acidity of the catalyst might decrease the probability of acid activation necessary to the formation of 1,3-PD. The reaction could be dominated by direct hydrogenolysis leading to the cleavage of the less sterically hindered primary C-O bond and, therefore, to the formation of 1,2-PD.

The effect of the reaction temperature was studied by testing several of the Ni-Cu bimetallic catalysts at different relative wt % of Ni and Cu at 453 K in order to evaluate the effect of Cu, less active metal, to control the formation of cracking gaseous products and the deep hydrogenation to carbonaceous materials that can be produced at higher reaction temperature. The consequences on the selectivity to 1,3-PD and 1,2-PD were also studied (Table 4). The types of products that were formed at 453 K were similar to those obtained at 393 K. The most important difference was observed on the product distribution. The diol selectivity decreased and the selectivity to propanol and dioxane or dioxolane increased for all catalysts when the reaction temperature was raised from 393 to 453 K (Table 3 and 4). However, an increase in the 1,3-PD/1,2-PD ratio was also observed for the catalysts used at 453 K compared to those tested at 393 K. In general, the selectivity to "others" was more significant when the reactions were carried out at higher temperature and with catalysts of high Cu wt % ratio. All catalysts displayed higher conversion at 453 K than at 393 K. The increase of activity was higher for the catalysts with higher wt % of Cu. The conversion values were comparable for Ni/S, NiCu(9:1)/S, NiCu(6:1)/S and NiCu(3:1)/S catalysts (99-92 %) (Table 4). The activity dropped to 82 and 75%, respectively for NiCu(1:3)/S and Cu/S. The diol selectivity decreased and the propanol selectivity increased at higher reaction temperature. This could be explained by over hydrogenolysis of the diols to propanol. Similar results were reported on diol over hydrogenolysis for supported Ni catalysts at comparable reaction temperature.[42] In contrast, for catalysts with lower metallic area and higher Cu wt % ratio, the Cu catalyzed deoxygenation pathway[32] resulted, initially, in the formation of acrolein, which upon hydrogenation gave propanol.

Dioxane and dioxolane were not observed for Ni/S catalyst both at 393 and 453 K suggesting that the acid catalyzed reactions were less important for the catalyst without copper, due to the higher activity of Ni. In contrast, the dioxane and dioxolane amounts were higher for the catalysts with lower metallic area (Table 4). Thermogravimetric-temperature programmed oxidation analysis (TG-TPO) of the spent catalysts revealed higher percentage of carbon deposition materials when the reaction was performed at 453 K and when the catalysts of higher amount of Cu were used (Table 5). This might suggest that the "others" products in this reaction were high molecular weight oligomerization products that could not be identified in the GC-MS analysis.

The 1,3-PD/1,2-PD ratio increased when increasing the reaction temperature for all catalysts (Table 4). For example, the 1,3-PD/1,2-PD ratio drastically increased from 0,17 at 393 K to 0,40 at 453 K for Ni/S. This might suggest that there was a shift in the mechanism leading to the formation of diols when

Table 5: N_2 physisorption and temperature programmed oxidation results of the spent catalysts.

Used catalyst	BET (m^2/g)	Pore volume (cc/g)	% organic deposition (TPO)
Ni/S-U[#]	157	0.20	n.d
NiCu(9:1)/S-U	155	0.20	1
NiCu(9:1)/S-U[#]	156	0.20	1
NiCu(6:1)/S-U	155	0.19	1
NiCu(6:1)/S-U[#]	153	0.20	3
NiCu(3:1)/S-U[#]	134	0.17	4
NiCu(1:1)/S-U	131	0.17	2
NiCu(1:3)/S-U	124	0.16	2
NiCu(1:3)/S-U[#]	110	0.15	7
Cu/S-U	130	0.14	2
Cu/S-U[#]	118	0.16	9
Ni-Cu(6:1)*/S-U[#]	101	0.15	1

[#] The results corresponds to the catalysts used at 453 K for 1 h whereas the rest of results are for the catalysts used at 393 K for 4 h.

the reaction temperature was increased. As we proposed earlier, the higher acid activity at 453 K could favor hydrogenolysis through a collaborative action between H^+ and metal sites favoring the formation of 1,3-PD. This ratio increased further when the wt % ratio of Cu increased suggesting that the acid catalyzed route is even more important at lower metallic area, which is responsible for the direct hydrogenolysis route.

A similar trend in conversion and selectivity was observed at higher reaction temperature when NiCu(6:1)*/S, with lower surface acidity and higher metallic area, was checked for comparison (Table 4). However, the diol selectivity was higher and the dioxane/ dioxolane selectivity was lower for this catalyst compared to NiCu(6:1)/S. This was in agreement with the higher metallic area and lower surface acidity of the former sample. Although the 1,3-PD/1,2-PD ratio increased for NiCu(6:1)*/S at higher reaction temperature, the value was lower than that of NiCu(6:1)/S meaning that the collaborative mechanism was less important for the former catalyst. This could be due to the combined effect of higher metallic area and lower surface acidity of this catalyst.

3.4. Characterization of spent catalysts

XRD pattern of the spent catalysts did not show significant variations with respect to those taken for the fresh catalysts. The N_2-adsorption results of the spent catalysts are presented in Table 5. Comparing these results with the corresponding values obtained for the catalyst precursors (Table 1), the spent catalysts, in general, had higher BET area and pore volume than their corresponding catalyst precursors. This could be due to a higher metal dispersion of the spent catalyst, which was also reported for a spent Cu catalyst supported on hectorite.[58] However, the spent catalysts with higher Cu wt % and tested at higher reaction temperature (453 K) exhibited lower BET area and pore volume. These results could be explained considering differences in the residual carbon compounds deposited on the catalyst surface during reaction. These differences were supported by the quantification of the coke formation by temperature programmed oxidation-thermogravimetric analysis of the spent catalysts (Table 5). The results showed lower percentage of deposited organic compounds for the samples with lower Cu wt % and for all catalysts used at lower reaction temperature.

Conclusions

Acid saponite supported Ni-Cu bifunctional catalysts were active for the hydrogenolysis of glycidol. We investigated the activity of the materials with different Ni-Cu ratios and reaction temperature. Characterization of the catalysts revealed the formation of a Ni-Cu alloy and a decrease in the metallic area, measured by hydrogen chemisorption, with the addition of Cu. This indicates that Ni and Cu are in intimate contact. The presence of Cu moderated the hydrogenation activity of Ni, decreasing the yield to diols, but increasing the selectivity towards 1,3 PD. These results suggest that Cu is required to modulate Ni activity and then promote the H^+-metal collaborative mechanism. At higher reaction temperature, the acid activation was improved, catalyzed reactions were promoted and, thus, the 1,3-PD/ 1,2-PD ratio increased. However, this increase in the reaction temperature with high Cu loading decreased the diol selectivity significantly and the selectivity for Cu catalyzed deoxygenation and acid catalyzed polymerization and oligomerization reaction products increased.

Author Contributions

Fiseha Bogale Gebretsadik: Investigation. Visualization. Writing-Original Draft; Javier Ruíz-Martínez: Validation. Supervision; María Dolores González: Conceptualization. Validation. Writing-Original Draft. Pilar Salagre: Conceptualization. Resources. Supervision. Yolanda Cesteros: Conceptualization. Resources. Supervision. Writing-Original Draft. Writing-Review & Editing.

Conflicts of interest

There are no conflicts to declare.

Acknowledgements

The authors are grateful for the financial support of the Ministerio de Economia y Competividad of Spain and FEDER funds (CTQ2011-24610) and the recognition from the Generalitat de Catalunya (2017 SGR 798).

Notes and references

1 A. J. Ragauskas, C. K. Williams, B. H. Davison, G. Britovsek, J. Cairney, C. A. Eckert, W. J. Frederick Jr., J. P. Hallett, D. J. Leak, C.L. Liotta, J.R. Mielenz, R. Murphy, R. Templer and T. Tschaplinski, *Science*, 2006, **311**, 484-489.
2 S. Fernando, S. Adhikari, C. Chandrapal and N. Murali, *Energy Fuels*, 2006, **20**, 1727-1737.
3 J. ten Dam and U. Hanefeld, *ChemSusChem*, 2011, **4**, 1017-1034.
4 A. Corma, S. Iborra and A. Velty, *Chem. Rev.*, 2007, **107**, 2411-2502.
5 G. W. Huber, S. Iborra and A. Corma, *Chem. Rev.*, 2006, **106**, 4044-4098.
6 E. van Ryneveld, A. S. Mahomed, P. S. van Heerden and H.B. Friedrich, *Catal Lett.*, 2011, **141**, 958-967.
7 M. Pagliaro, R. Ciriminna, H. Kimura, M. Rossi and C. D. Pina, *Angew. Chem. Int. Ed.*, 2007, **46**, 4434-4440.
8 C. H. C. Zhou, J. N. Beltramini, Y. X. Fan and G. Q. M. Lu, *Chem. Soc. Rev*., 2008), **37**, 527-549.
9 A. Behr, J. Eilting, K. Irawadi, J. Leschinski and F. Lindner, *Green Chem.*, 2008, **10**, 13-30.
10 L. Z. Qin, M. J. Song and C. L. Chen, *Green Chem.*, 2010, **12**, 1466-1472.
11 G. A. Kraus, *Clean-Soil Air Water*, 2008, **36**, 648-651.
12 J. Chaminand, L. Djakovitch, P. Gallezot, P. Marion, C. Pinel and C. Rosier, *Green Chem.*, 2004, **6**, 359-361.
13 P. N. Caley and R. C. Everett, US Patent 3350871, 1967.
14 D. Zimmerman and R. B. Isaacson, US Patent 3814725, 1974.
15 M. Akiyama, S. Sato, R. Takahashi, K. Inui and M. Yokota, *Appl. Catal. A: Gen.*, 2009, **371**, 60-66.

16 I. Gandarias, P. L. Arias, J. Requies, M. B. Güemez, J. L. G. Fierro, *Appl. Catal. B: Environ.*, 2010, **97**, 248-246.
17 Y. Nakagawa, M. Tamura and K. Tomishige, *J. Mater. Chem. A*, 2014, **2**, 6688-6702.
18 L. Gong, Y. Lu, Y. Ding, R. Lin, J. Li, W. Dong, T. Wang and W. Chen, *Appl Catal., A: Gen.*, 2010, **390**, 119-126.
19 Y. Nakagawa, Y. Shinmi, S. Koso and K. Tomishige, *J. Catal*., 2010, **272**, 191-194.
20 J. Wang, M. Yang and A. Wang, *Chin. J. Catal.*, 2020, **41**, 1311–1319.
21 Y. Liang, G. Shi and K. Jin, *Catal. Lett*., 2020, **150**, 2365–2376.
22 W. Zhou, Y. Li, X. Wang, D. Yao, Y. Wang, S. Huang, W. Li, Y. Zhao, S. Wang and X. Ma, *J. Catal.*, 2020, **388**, 154–163.
23 Z. Xi, Z. Hong, F. Huang, Z. Zhu, W. Jia and J. Li, *Catalysts*, 2020, **10**, 312.
24 J. W. Yoo, Z. Mouloungui and A. Gaset, US Patent 6316641, 2001.
25 R. Bai, H. Zhang, F. Mei, S. Wang, T. Li, Y. Gu and G. Li, *Green Chem.,* 2013, **15**, 2929-2934.
26 D. Cespi, R. Cucciniello, M. Ricciardi, C. Capacchione, I. Vassura, F. Passarini and A. Proto, *Green Chem.* 2016, **18**, 4559-4570.
27 A. Fási, I. Pálinkó and I. Kiricsi, *J. Catal.*, 1999, **188**, 385-392.
28 A. Fási, I. Pálinkó and I. Kiricsi, *Stud. Surf. Sci. Catal.*, 2000, **130**, 839-844.
29 I. Salla, O. Bergadà, P. Salagre, Y. Cesteros, F. Medina, J. E. Sueiras and T. Montanari, *J. Catal.*, 2005, **232**, 239–245.
30 A. Fási, I. Pálinkó, K. Hernadi and I. Kiricsi, *Catal. Lett.*, 2002, **81**, 237-240.
31 M. Bartók, A. Fási and F. Notheisz, *J. Catal.*, 1998, **175**, 40-47.
32 M. Bartók, A. Fási and F. Notheisz, *J. Mol. Catal. A: Chem.*, 1998, **135**, 307-316.
33 S. Koso, I. Furikado, A. Shimao, T. Miyazawa, K. Kunimori and K. Tomishige, *Chem. Comm.*, 2009, 2035-2037.
34 S. Koso, N. Ueda, Y. Shinmi, K. Okumura, T. Kizuka and K. Tomishige, *J. Catal.*, 2009, **267**, 89-92.
35 K. Chen, S. Koso, T. Kubota, Y. Nakagawa and K. Tomishige, *ChemCatChem*, 2010, **2**, 547-555.
36 K. Chen, K. Mori, H. Watanabe, Y. Nakagawa and K. Tomishige, J. Catal., 2012, **294**, 171-183.
37 M. Chia, Y. J. Pagán-Torres, D. D. Hibbitts, Q. Tan, H. N. Pham, A. K. Datye, M. Neurock, R. J. Davis, J. A. Dumesic, *J. Am. Chem. Soc.,* 2011, **133**, 12675-12689.
38 L. Ye, X. Duan, H. Lin and Y. Yuan, *Catal. Today*, 2012, **183**, 65-71.
39 U. Saxena, N. Dwivedi and S. R. Vidyarthi, *Ind. Eng. Chem. Res.*, 2005, **44**, 1466-1473.
40 L. Zhou, A. Wang, C. Li, M. Zheng and T. Zhang, *ChemSusChem*, 2012, **5**, 932-938.
41 F. B. Gebretsadik, J. Ruiz-Martinez, P. Salagre and Y. Cesteros, *Appl. Catal. A: Gen.,* 2017, **538**, 91-98.
42 F. B. Gebretsadik, J. Llorca, P. Salagre and Y. Cesteros, *ChemCatChem*, 2017, **9**, 3670-3680.
43 Y. Sun, Z. Cai, X. Li, P. Chen and Z. Hou, *Catal. Sci. Technol*, 2019, **9**, 5022-5030.
44 V. Ponec, *Appl. Catal. A: Gen.,* 2001, **222**, 31-45.
45 I. Gandarias, S. G. Fernández, M. El Doukkali, J. Requies and P. L. Arias, *Top. Catal.*, 2013, **56**, 995-1007.
46 S. Sato, M. Akiyama, R. Takahashi, T. Hara, K. Inui and M. Yokota, *Appl. Catal. A: Gen.*, 2008, **347**, 186–191.
47 P. Li, J. Liu, N. Nag and P.A. Crozier, *J. Catal.,* 2009, **262**, 73-82.
48 F.B. Gebretsadik, D. Mance, M. Baldus, P. Salagre and Y. Cesteros, *Appl. Clay Sci.,* 2015, **114**, 20-30.
49 R. Mokaya, W. Jones, S. Moreno and G. Poncelet, *Catal. Lett.*, 1997, **49**, 87-94.
50 A. Carrero, J.A. Calles and A.J. Vizcaíno, *Chem. Eng. J.,* 2010, **163**, 395-402.
51 J.-P. Shen and C. Song, *Catal. Today,* 2002, **77**, 89-98.
52 F.E. López-Suárez, A. Bueno-López and M.J. Illán-Gómez, *Appl. Catal. B: Environ.*, 2008, **84**, 651-658.
53 I. Obregón, E. Corro, U. Izquierdo, J. Requies and P.L. Arias, *Chin. J. Catal*., 2014, **35**, 656-662.
54 A. West, *Solid State Chemistry and its Application*, John Wiley & Sons, New York, 1985.
55 A. Kitla, O.V. Safonova and K. Föttinger, *Catal. Lett*., 2013, **143**, 517-530.
56 J. Batista, A. Pintar, J.P. Gomilšek, A. Kodre and F. Bornette, *Appl. Catal. A: Gen.,* 2001, **217**, 55-68.
57 B. C. Miranda, R. J. Chimentão, J. Szanyi, A. H. Braga, J. B. O. Santos, F. Gispert-Guirado, J. Llorca, F. Medina, *Appl. Catal. B: Environ.*, 2015, **166–167**, 166-180.
58 T. Sánchez, P. Salagre, Y. Cesteros and A. Bueno-López, *Chem. Eng. J.*, 2012, **179**, 302- 311.